



20 **ABSTRACT**

21 The importance of the textural and physicochemical characteristics upon the adsorption  
22 capacity of the commercial activated carbons (ACs) Coconut, Wood, Merck, Darco and Norit  
23 towards ronidazole (RNZ) and diclofenac (DCF) from water solution was investigated  
24 thoroughly in this work. At pH = 7, Coconut AC and Wood AC presented the highest  
25 adsorption capacity towards RNZ (444 mg/g) and DCF (405 mg/g). The maximum mass of  
26 RNZ adsorbed onto Coconut AC was higher in this study than those outlined previously in  
27 other works. Besides, the maximum capacity of Wood AC for adsorbing DCF was  
28 comparable to those found for other ACs. The adsorption capacity of all the ACs was  
29 increased by surface area and was favored by incrementing the acidic site concentration. The  
30  $\pi$ - $\pi$  stacking interactions were the predominant adsorption mechanism for the RNZ and DCF  
31 adsorption on ACs, and the acidic sites favored the adsorption capacity by activating the  $\pi$ - $\pi$   
32 stacking. Electrostatic interactions did not influence the adsorption of RNZ on Coconut AC,  
33 but electrostatic repulsion decreased that of DCF on Wood AC. The adsorption of DCF on  
34 Wood AC was reversible but not that of RNZ on Coconut AC. Besides, the adsorption of  
35 RNZ and DCF on the Coconut and Wood ACs was endothermic in the range of 15-25 °C.

36

37

38

39 **Keywords:** Activated carbon, adsorption mechanism, diclofenac, ronidazole, surface  
40 chemistry.

41

42

43

## 44 1. INTRODUCTION

45 The excessive utilization of pharmaceuticals in animal and human health care has  
46 originated that considerable amounts of drugs are being discharged to the aquatic  
47 environment (surface, drinking and ground waters), sediments, soil, and food chains (Wang  
48 and Wang 2016). Effluents from municipal wastewater treatment plants release  
49 pharmaceutical compounds into surface water sources since the existing biological water  
50 treatment processes do not successfully remove these compounds. Antibiotics and anti-  
51 inflammatories are some of the most commonly detected organic microcontaminants in  
52 municipal wastewater, posing a disturbing hazard since these compounds are toxic even at  
53 trace levels (Halling-Sørensen et al. 1998; Jeon and Hollender 2019; Ternes and Hirsch  
54 2000).

55 Antibiotics are broadly prescribed to prevent or treat microbial infections, and several  
56 of them are recalcitrant or difficult to decompose in aerobic biological treatment processes  
57 (Kümmerer 2009). Distinct antibiotics were found in the hospital residual waters, industrial  
58 and municipal wastewater and surface water. Amoxicillin (900-9940 ng/L) (Watkinson et al.  
59 2009), ampicillin (5800 ng/L) (Lin et al. 2008), cephalexin (3100-64000 ng/L) (Watkinson  
60 et al. 2009), ciprofloxacin (11-15000 ng/L) (Spongberg and Witter 2008; Watkinson et al.  
61 2009), sulfamethoxazole (4-9460 ng/L) (Díaz-Cruz et al. 2008) and tetracycline (15000 ng/L)  
62 (Lin et al. 2008) are some of the antibiotics detected in water resources.

63 Notwithstanding, the nonsteroidal anti-inflammatory pharmaceuticals (NSAIDs) are  
64 being widely prescribed for curing dysmenorrhea fever, headaches, inflammatory  
65 arthropathy, osteoarthritis and rheumatoid arthritis, among others (Richard et al. 2007).  
66 These anti-inflammatories have been found not only in surface waters but also in residual  
67 waters. Among the NSAIDs frequently detected in water are acetaminophen (211 ng/L)

68 (Santos et al. 2013), diclofenac (60-1900 ng/L) (Gómez et al. 2007), famotidine (94 ng/L)  
69 (Lin et al. 2008) and ibuprofen (300 ng/L) (Lin and Tsai 2009).

70 Various processes have been applied to eliminating pharmaceutical compounds in  
71 water. Among these, advanced oxidation processes, adsorption, photodegradation, soil  
72 sorption, electrochemical degradation and biosorption by aquatic plants are being  
73 successfully applied lately (Chianese et al. 2016; Moral-Rodriguez et al. 2016; Martínez-  
74 Costa et al. 2020).

75 Adsorption is a separation process that has attracted considerable attention due to the  
76 low operating costs and availability of different adsorbents. Different activated carbons  
77 (ACs) have been prepared for removing various drugs from water solutions. Malhotra et al.  
78 (Malhotra et al. 2018) examined the adsorption of diclofenac (DCF) on an AC synthesized  
79 by chemical activation of tea residues using  $ZnCl_2$ ,  $K_2CO_3$ , KOH and  $H_2SO_4$ , denoted as  
80 AC1, AC2, AC3 and AC4, correspondingly. The adsorption capacity decreased in the  
81 following order:  $AC1 > AC2 > AC3 > AC4$ ; likewise, the surface diminished in the same  
82 order.

83 Recently, the adsorption capacity of a commercial AC towards DCF was enhanced  
84 by modifying the commercial AC using chemical activation with  $CO_2$ , and the adsorption  
85 capacity was raised nearly linearly with the AC surface area (Moral-Rodríguez et al. 2019).  
86 In another work, ACs were synthesized from sewage sludge that was mixed with a  $ZnCl_2$   
87 solution, using different ratios of  $ZnCl_2$ /sludge (0.5, 1.0, and 1.5) and carbonized at different  
88 temperatures (500, 650 and 800 °C) (dos Reis et al. 2016). These ACs were applied to remove  
89 nimesulide (NM) and DCF in a water solution, and the maximum mass of NM and DCF  
90 adsorbed was 66.4 and 157.4 mg/g, correspondingly.

91 Moral-Rodríguez et al. (2016) researched for eliminating ronidazole (RNZ) and  
92 sulfamethoxazole (SMX) from a water solution by adsorption on a commercial AC,  
93 designated as F400. The findings disclosed that the adsorption of SMX on F400 relied on the  
94 temperature, ionic strength, pH and aqueous matrix, whereas the operating conditions did not  
95 change the adsorption of RNZ on F400. Furthermore, the uptake of RNZ adsorbed on F400  
96 was higher (352.26 - 518.39 mg/g) than that of SMX (126.64 - 445.77 mg/g). It was also  
97 demonstrated that the F400 capacity towards RNZ and SMX was significantly dependent  
98 upon its textural properties and the molecular size of each antibiotic.

99 Although the effectiveness of adsorption on carbonaceous materials for eliminating  
100 pharmaceutical compounds in aqueous solution has been extensively analyzed. **The novelty**  
101 **of this work is to study the relationship between the adsorption capacity of activated carbon**  
102 **and their chemical and textural properties.** Therefore, this study's principal goal was to  
103 analyze the adsorption equilibrium of DCF and RNZ on five commercial ACs having  
104 different **chemical and textural characteristics.** Besides, the dependence of the adsorption  
105 capacities of these ACs regarding **solution pH and temperature** was investigated in detail.  
106 Moreover, the adsorption mechanisms of RNZ and DCF on the ACs were explained **and the**  
107 **reversibility of the adsorption and reuse of ACs were also examined in this work.**

108

## 109 **2. EXPERIMENTAL METHODOLOGY**

### 110 **2.1 Adsorbents and characterization**

111 Five commercial ACs were used and were designated as Coconut, Wood, Merck,  
112 Darco and Norit. The ACs were pretreated by washing with water, drying in an electric oven  
113 overnight ( $T = 120\text{ }^{\circ}\text{C}$ ), sieving and storing in a sealed vessel. The particles of ACs have a  
114 mean diameter of 0.056 mm.

115 The textural properties of ACs, namely surface area ( $S_{\text{BET}}$ ), pore volume ( $V_{\text{P}}$ ), and  
116 average pore diameter ( $d_{\text{P}}$ ), were assessed from the adsorption-desorption isotherm of  $\text{N}_2$ ,  
117 which was measured in a physisorption apparatus, Micromeritics, ASAP 2020. The  
118 determination of  $S_{\text{BET}}$  was carried out by the method proposed by Brunauer, Emmett, and  
119 Teller (BET) (Brunauer et al. 1938). The Dubinin-Radushkevich (DR) isotherm (Rouquerol  
120 et al. 2014) was applied to evaluate the micropore volume ( $V_{\text{mic}}$ ), specific micropore area  
121 ( $S_{\text{mic}}$ ) and average micropore width ( $L_0$ ). Lastly, the pore size distribution of each AC was  
122 computed using the density functional theory. The basic and acidic sites concentrations on  
123 the AC surface were ascertained by Boehm's titration method (Boehm 1966); otherwise, the  
124 surface charge of the adsorbents was assessed by the acid-base titration technique developed  
125 by Babic et al. (1999).

## 126 **2.2 Technique for procuring the adsorption data of RNZ and DCF**

127 The pharmaceutical compounds employed in this study were ronidazole (RNZ) and  
128 diclofenac sodium (DCF), supplied by Merck. Table 1 displays the chemical characteristics  
129 and molecular structure of RNZ and DCF. The molecular **structure** of each **compound** was  
130 obtained by applying the hybrid density functional b3lyp. Fig. 1a and 1b show the speciation  
131 diagrams for RNZ and DCF in water solutions, calculated using the corresponding  
132 dissociation constants (see Table 1).

133 The determination of RNZ and DCF was performed by UV-Visible  
134 spectrophotometry. The calibration curves for RNZ and DCF were prepared from standard  
135 solutions having concentrations from 100 to 1000 mg/L. A spectrophotometer, Shimadzu  
136 (model UV 2600), was employed to determine the absorbances of RNZ and DCF solutions  
137 **at wavelengths of 309 and 276 nm**, correspondingly, and the calibration curves were made at  
138 the particular pH of the RNZ and DCF sample solutions.

139 A solution with an ionic strength (0.01 N) and a specific pH was fixed by combining  
140 appropriate volumes of 0.01 N HCl and NaOH solutions. This constant ionic strength solution  
141 was employed for fixing all RNZ and DCF solutions, having initial concentrations varying  
142 from 100 to 1000 mg/L.

143 The data for the RNZ and DCF adsorption on the ACs were obtained in an  
144 experimental adsorber operated in batch mode. An AC mass of 50 mg and 40 mL of the RNZ  
145 or DCF solutions of different initial concentrations were added into 50 mL Falcon tubes  
146 (adsorber). Afterward, the Falcon tube was set down in a thermostatic bath, allowing the  
147 solution and ACs to reach adsorption equilibrium. In preliminary tests, the concentration of  
148 the pharmaceuticals in solution was monitored daily, and the concentration did not change  
149 after 5 days so that 7 days was sufficient time to approach equilibrium. Three times daily, the  
150 adsorber solutions were mechanically shaken for 15 min by placing the adsorbers on top of  
151 an Orbital Shaker TS-100. Posterior to 7 days, a solution was taken out and analyzed by the  
152 analytical method detailed above to quantify the equilibrium concentration of the  
153 pharmaceutical.

154 At  $T = 25\text{ }^{\circ}\text{C}$ , the dependence of the adsorption equilibrium on pH was analyzed by  
155 procuring the adsorption data at pH of 3, 7 and 11 for RNZ and pH of 6, 7, 9 and 11 for DCF.  
156 In all the experimental runs, few drops of HCl and NaOH solutions of 0.01 N were  
157 supplemented to keep the solution pH constant. Moreover, the temperature influence was  
158 analyzed by measuring the adsorption equilibrium data at 35, 25, and 15  $^{\circ}\text{C}$  and  $\text{pH} = 7$ . The  
159 mass adsorbed of RNZ and DCF on the carbons was appraised by conducting a mass balance  
160 of the pharmaceutical in the batch adsorber, expressed as follows:

$$q = \frac{V(C_0 - C_e)}{m} \quad (1)$$

161 Where  $q$  denotes the mass of RNZ or DCF adsorbed at equilibrium (mg/g),  $V$  represents the  
162 volume of the RNZ or DCF solutions (L),  $C_0$  is the initial concentration of the RNZ or DCF  
163 (mg/L),  $C_e$  is the equilibrium concentration of RNZ or DCF (mg/L), and  $m$  is AC mass (g).

### 164 **2.3 Technique for conducting the desorption and reuse experiments**

165 The desorption and reuse experiments of the pharmaceutical compounds were  
166 evaluated by conducting an adsorption-desorption-re-adsorption cycle. Firstly, at  $T = 25\text{ }^\circ\text{C}$   
167 and  $I = 0.01\text{ N}$ , the adsorption of DCF on Wood AC at  $\text{pH} = 6$  and RNZ on Coconut AC at  
168  $\text{pH} = 7$  were conducted as described above. The Wood and Coconut ACs were chosen  
169 because they presented the highest adsorption capacity towards DCF and RNZ. The AC  
170 equilibrated with the pharmaceutical compound was extracted from the solution, rinsed with  
171 20 mL of deionized water for 5 min to remove the pharmaceutical not adsorbed, and the  
172 rinsing water was decanted. Then, AC was subsequently transferred into another adsorber  
173 holding a solution without the pharmaceutical compound (40 mL) with  $I = 0.01\text{ N}$  and  $\text{pH} =$   
174 11 for DCF and  $\text{pH} = 7$  for RNZ. The  $\text{pH}$  was measured and adjusted periodically to keep it  
175 constant, as described above. Upon reaching desorption equilibrium (eight days), the solution  
176 was sampled, and the concentration of the pharmaceutical compound was determined as  
177 described above. The amount of pharmaceutical not desorbed was computed as follows:

$$q_{\text{des,e}} = q_0 - \frac{V}{m} C_{\text{des,e}} \quad (2)$$

178 where  $C_{\text{des,e}}$  is the concentration of the pharmaceutical compound at equilibrium in the  
179 desorption experiment, mg/L;  $q_0$  is the uptake of the pharmaceutical already adsorbed at the  
180 starting of the desorption experiment, mg/g;  $q_{\text{des,e}}$  represents the equilibrium uptake of the  
181 pharmaceutical that did not desorb in the desorption run, mg/g.



182 After the desorption experiment, the AC was extracted from the solution, rinsed with  
183 deionized water as described previously and designated as regenerated AC. Then, the  
184 regenerated AC was added into a batch adsorber to perform an adsorption experiment, and  
185 the re-adsorption capacity of the regenerated AC,  $q_{\text{ReAd}}$ , was calculated by equation (1).

186 The re-adsorption efficiency (%RE) of the ACs for a new cycle of adsorption was  
187 calculated using the subsequent equation:

$$\%RE = \frac{q_{\text{ReAd}}}{q} \times 100 \% \quad (3)$$

188

### 189 3. RESULTS AND DISCUSSION

#### 190 3.1 Properties of Commercial ACs

191 The textural characteristics  $S_{\text{BET}}$ ,  $V_{\text{p}}$ ,  $d_{\text{p}}$ ,  $V_{\text{mic}}$ ,  $L_0$ , and  $S_{\text{mic}}$  of all ACs are registered  
192 in Table 2. The  $S_{\text{BET}}$  of the ACs decreased from 1357 to 510  $\text{m}^2/\text{g}$ , and the decreasing order  
193 is as follows: Wood > Merck > Coconut > Norit > Darco. Furthermore, the total  $V_{\text{p}}$  was  
194 evaluated at  $(P/P_s) = 0.99$  and varied from 0.44 to 1.18  $\text{cm}^3/\text{g}$ , showing that the porosity of  
195 the ACs changed broadly.

196 The adsorption-desorption isotherms of  $\text{N}_2$  on the ACs are plotted in Fig. S.1.  
197 According to the classification recommended by IUPAC (Rouquerol et al. 2014), the  
198 isotherm shapes of Coconut and Merck ACs are type Ia (Fig. S.1 a) and Ib (Fig. S.1 b),  
199 respectively. These isotherms are reversible and have a high opening in the adsorption  
200 shoulder, which is characteristic of microporous materials. For the isotherm Ia, the type of  
201 microporosity is narrower if compared to that of isotherm Ib, where the diameters of the  
202 micropores are wider according to the opening of the adsorption shoulder (see isotherm Ib).  
203 The adsorption isotherms of the Darco, Norit, and Wood ACs have shapes of type IIb (Fig.

204 S.1 c, d, and e), distinctive of mesoporous materials, showing the hysteresis loops H<sub>3</sub> and H<sub>4</sub>  
205 type. The hysteresis loop H<sub>3</sub> (Fig. S.1 c) often occurs in materials formed by aggregates of  
206 particles with sheet morphology, while the H<sub>4</sub> (Fig. S.1 d and e) is typical of activated carbons  
207 and other adsorbents, which have slit shape pores and high distribution of micropores  
208 (Boehm 1966).

209 The V<sub>mic</sub> of the Coconut, Merck, Norit, Darco and Wood ACs represented 86, 58, 51,  
210 36 and 34 % of the total V<sub>p</sub>, respectively, confirming that the Coconut and Merck ACs  
211 consisted mainly of micropores.

212 Fig. S.2 displays the cumulative pore volume and distribution of pore size for all ACs.  
213 The accumulated pore volume distribution of the Coconut AC (see Fig. S.2 a) shows that the  
214 volume of micropores is 94.3 % of the entire pore volume, although the remaining 5.7 % is  
215 mesoporous. Furthermore, the pore size distribution is almost unimodal, and the approximate  
216 pore diameter was about 0.65 nm. Likewise, in Fig. S.2 e, the cumulative volume distribution  
217 of the Wood AC revealed that the micropores and mesopores represented 49 and 51 % of the  
218 total pore volume, correspondingly. On the other hand, it can be corroborated that most of  
219 the micropore sizes are between 0.5 and 0.75 nm for Coconut AC and varying from 0.65 to  
220 0.75 nm for the Wood AC.

221 Table 3 shows that the concentrations of the total basic and acid sites for the ACs  
222 varied from 0.093 to 4.995 meq/g and 0.093 to 1.874 meq/g, respectively. As can be seen,  
223 the total acidic and basic sites concentrations ranged widely. The Wood AC surface exhibited  
224 a more acidic character (pH<sub>PZC</sub> = 3.64), considering that the concentration of acidic sites was  
225 7.7 times larger than that of the basic ones. Otherwise, the concentration of basic sites of  
226 Coconut AC was 7-fold larger than those of acid sites (pH<sub>PZC</sub> = 10.85). In general, the acid  
227 sites concentrations of the ACs decreased as follows: Wood > Coconut > Norit > Darco >

228 Merck, whereas the basic sites diminished in the subsequent order: Coconut > Norit > Wood  
 229 > Merck  $\approx$  Darco.

### 230 3.2 Modeling the adsorption data of RNZ and DCF

231 The adsorption isotherms of Freundlich, Langmuir and Prausnitz-Radke (P-R)  
 232 interpreted the data for the adsorption equilibrium of both pharmaceuticals. These isotherm  
 233 models are mathematically expressed as follows (Leyva-Ramos 2007):

$q = kC^n$	(4)
$q = \frac{q_m KC}{1+KC}$	(5)

$$q = \frac{aC}{1+bC^\beta} \quad (6)$$

234 Where  $a$  (L/g),  $b$  (L <sup>$\beta$</sup> /mg <sup>$\beta$</sup> ) and  $\beta$  are the Prausnitz-Radke model constants,  $C$  (mg/L) denotes  
 235 the equilibrium concentration of pharmaceutical,  $k$  (mg<sup>1-1/n</sup>L<sup>1/n</sup>/g) and  $n$  designate the  
 236 Freundlich model constants,  $K$  (L/mg) and  $q_m$  (mg/g) are the Langmuir isotherm parameters  
 237 associated with the adsorption heat and the maximum mass of pharmaceutical adsorbed on  
 238 ACs, respectively, and  $q$  (mg/g) represents the equilibrium amount adsorbed of  
 239 pharmaceutical.

240 The parameters for adsorption isotherms were calculated by matching the adsorption  
 241 models to the data using a nonlinear regression method based upon the Rosenbrock-Newton  
 242 optimization algorithm. Besides, the average percent deviation for each adsorption model,  
 243 %D, was appraised using the succeeding mathematical relationship:

$$\%D = \left( \frac{1}{N} \sum_{i=1}^N \left| \frac{q_{\text{exp}} - q_{\text{pred}}}{q_{\text{exp}}} \right| \right) \times 100 \% \quad (7)$$

244 Tables 4 and 5 list the parameters and %D for the P-R isotherm, and the parameters  
 245 and %D for the Langmuir and Freundlich isotherms are registered in Tables S1, S2 and S3.

246 The %D values for the R-P isotherm model were shorter than the %D values of the Freundlich  
247 and Langmuir adsorption models in 22 out of the 28 experimental conditions registered in  
248 Tables 4, 5, S1, S2 and S3. Therefore, the P-R model better interpreted the experimental data  
249 since it is a three-parameter isotherm, while the Langmuir and Freundlich isotherms are two-  
250 parameter adsorption models. The P-R adsorption model adequately represented the  
251 experimental data since the %D varied from 0.9 to 21.0 %.

### 252 3.3 Adsorption of RNZ and DCF on ACs

253 At  $T = 25\text{ }^{\circ}\text{C}$  and  $\text{pH} = 7$ , the isotherms of RNZ and DCF adsorbed on ACs are shown  
254 in Fig. 2a and 2b. As depicted in Fig. 2a, the capacities of ACs for adsorbing RNZ in water  
255 solution diminished as follows: Coconut > Wood > Norit > Merck > Darco. At the RNZ  
256 equilibrium concentration of 500 mg/L, the uptake of RNZ adsorbed ( $q_{500}$ ) upon the Coconut,  
257 Wood, Norit, Merck and Darco is 434, 350, 283, 261 and 188 mg/g, respectively. It can be  
258 noted that Coconut and Darco presented the largest and lowest adsorption capacity towards  
259 RNZ. In Fig. 2b, it is observed that Wood had the highest adsorption capacity towards DCF.  
260 The  $q_{500}$  for DCF on the Wood, Merck, Coconut, Norit and Darco is 396, 248, 222, 182 and  
261 166 mg/g, correspondingly, so that the AC capacities for adsorbing DCF decreased in the  
262 subsequent series: Wood > Merck > Coconut > Norit > Darco. It is worth mentioning that  
263 the  $S_{\text{BET}}$  values of ACs decreased in the same order as their adsorption capacities towards  
264 DCF (See Table 2).

265 In this work, the maximum uptake of RNZ adsorbed on Coconut AC was 444 mg/g  
266 at pH of 7 and T of 25 °C and was slightly larger than those presented in previous studies  
267 (Méndez-Díaz et al. 2010; Moral-Rodríguez et al. 2016). The maximum adsorption capacities  
268 of three commercial carbons towards RNZ ranged from 376 to 394 mg/g (Méndez-Díaz et  
269 al. 2010; Moral-Rodríguez et al. 2016). While the Wood AC presented the maximum uptake

270 of DCF adsorbed of 441 mg/g, which is within the range (47.12-1033 mg/g) found for the  
271 adsorption capacities of pristine and modified ACs (Moral-Rodriguez et al. 2019; Viotti et  
272 al. 2019).

273 Fig. 3 depicts the molar uptake of DCF and RNZ adsorbed for the concentration at  
274 equilibrium of 500 mg/g,  $Q_{500}$  (mmol/g), graphed vs. the BET surface area of the AC. It can  
275 be noticed that the capacity of ACs for DCF incremented approximately linearly by  
276 augmenting  $S_{BET}$  and this result was expected because the adsorption capacities of the ACs  
277 decreased in same order as the  $S_{BET}$ . In the case of RNZ, the capacity of ACs for adsorbing  
278 RNZ increased somehow linearly with surface area, except for the Coconut AC. The finding  
279 that the surface area affected the adsorption capacity corroborated that the  $\pi$ - $\pi$  dispersive  
280 interactions were the predominant adsorption mechanism. These interactions are related to  
281 the  $\pi$  electrons of the aromatic ring of RNZ or DCF and the  $\pi$  electrons existing in the AC  
282 graphene planes and the  $S_{BET}$  is directly related to the AC graphene planes. The Coconut AC  
283 had the greatest adsorption capacity towards RNZ, but the Coconut AC did not have the  
284 highest  $S_{BET}$  and was the AC having the largest concentration of basic sites. This result  
285 demonstrated that the surface chemistry of ACs could also affect their adsorption capacity.

286 The molar  $Q_{500}$  of RNZ was always higher than that of DCF independently of the AC.  
287 This result can be ascribed to the molecular dimensions of RNZ (Table 1), which are shorter  
288 than those of DCF so that the RNZ molecules can access more micropores than the DCF  
289 molecules, and more adsorption sites are available for adsorbing RNZ.

290 The molar  $Q_{500}$  for RNZ and DFC vs. the concentration of acidic sites per unit surface  
291 area of AC (acidic sites/ $S_{BET}$ ) are plotted in Fig. 4. Overall, the acidic sites concentration  
292 promoted the adsorption capacity of ACs. Except for Merck AC, the capacities of the ACs  
293 for adsorbing DCF were raised linearly by increasing the concentration of acidic sites. Again,

294 the Coconut AC exhibited the highest molar  $Q_{500}$  for RNZ, but this carbon did not have the  
295 largest concentration of acidic sites. The acidic site concentration favored the AC adsorption  
296 capacity because some of the acidic sites can activate the  $\pi$ - $\pi$  dispersion interactions  
297 (Carrales-Alvarado et al. 2014). The preceding results corroborated that the ACs adsorption  
298 capacities towards RNZ and DCF from water solutions are significantly dependent on the  
299 textural and chemical characteristics of ACs.

### 300 3.4 Influence of pH on the capacity of Coconut AC for adsorbing RNZ

301 The dependence of the Coconut AC capacity for RNZ on the pH is exhibited in Fig.  
302 5, and the adsorption capacity rises marginally by augmenting the pH from 3 to 7; however,  
303 at pH = 11, the adsorption of RNZ on Coconut AC was significantly enhanced when the  
304 concentrations of RNZ at equilibrium were higher than 200 mg/L. For the RNZ concentration  
305 of 300 mg/L, the RNZ uptakes at pH of 3, 7, and 11 were 364, 389, and 548 mg/g,  
306 respectively. Therefore, the mass of RNZ adsorbed at pH = 11 was 1.5 and 1.4-fold higher  
307 than those at pH of 3 and 7, respectively.

308 The above results can be rationalized according to the speciation diagram of RNZ  
309 (Fig. 1), which indicates that in the pH range of 3-9, the RNZ molecule exists as the  
310 undissociated species, and the surface of the Coconut AC is positively charged ( $pH_{PZC} =$   
311 10.85). Hence, in this pH range, the electrostatic interactions did not influence the adsorption  
312 of RNZ, confirming that the RNZ is adsorbed on Coconut AC by  $\pi$ - $\pi$  interactions mainly.  
313 Although the surface of the Coconut AC is now slightly negatively charged at pH = 11, and  
314 the RNZ is still present as the neutral species, corroborating that the electrostatic interactions  
315 did not affect the RNZ adsorption. However, at pH = 11, the adsorption capacity increased  
316 for concentrations higher than 100 mg/L. This increase was due to the reduction of the RNZ  
317 solubility at basic pH since the solubility of non-polar organic compounds diminishes in the

318 presence of salts (Carrales-Alvarado et al. 2014). At pH = 11, the concentration of Na<sup>+</sup> ions  
319 is augmented because of the addition of NaOH solution to adjust the solution pH.  
320 Consequently, the hydrophobic interactions between the RNZ and the water favored the  
321 accumulation of RNZ on the the surface of the Coconut AC. Hence, the adsorption of RNZ  
322 en Coconut AC at pH = 11 is related to the  $\pi$ - $\pi$  dispersive interactions and hydrophobic  
323 interactions.

### 324 3.5 Influence of pH on the capacity of Wood AC for adsorbing DCF

325 Fig. 6 illustrates the pH influence on the capacity of Wood AC for adsorbing DCF.  
326 The adsorption capacity diminished considerably and moderately by incrementing the pH  
327 from 6 to 9 and 9 to 11, correspondingly. None adsorption runs were performed at pH < 6  
328 because the DCF solubility in water is low (Llinàs et al. 2007). For a DCF equilibrium  
329 concentration of 300 mg/L, the uptake of DCF adsorbed was 568, 353, 278 and 244 mg/g for  
330 the pH values of 6, 7, 9 and 11, correspondingly. The capacity of Wood AC at pH = 6 was  
331 1.6, 2.0 and 2.3 times higher than those at pH of 7, 9 and 11.

332 The above behavior can be ascribed to the fact that the DCF molecules in water are  
333 the anionic species (DCF<sup>-</sup>) in the pH span from 6 to 11, while the surface of Wood AC is  
334 negatively charged (pH<sub>PZC</sub> = 3.64). Thus, the lessening of the adsorption capacity was  
335 associated with the increment of the electrostatic repulsion existing between the negatively  
336 charged surface of the Wood AC and anionic DCF<sup>-</sup> because the negative charge of AC  
337 surface augments by raising the pH.

338 The influence of the electrostatic interactions in the DCF adsorption mechanism on  
339 Wood AC was further analyzed by carrying out adsorption runs at the solution ionic strengths  
340 of 0.01, 0.1 and 1.0 N (Moral-Rodriguez 2019). The results (not shown in this work)  
341 demonstrated that the capacity of Wood AC for adsorbing DCF increased while raising the

342 ionic strength. The ionic strength was varied by changing the NaCl concentration in the  
343 solution, so the Na<sup>+</sup> ions adsorb on the AC negative surface, balancing the negative charge  
344 of the AC and decreasing the repulsion between DCF<sup>-</sup> and the Wood AC surface, enhancing  
345 the adsorption of DCF. This effect is known as the screening effect (Moreno-Castilla 2004).

### 346 **3.6 Desorption of pharmaceutical compounds and reuse of regenerated AC**

347 The reversibility of the adsorption of RNZ on Coconut AC and DCF on Wood AC  
348 was investigated by performing adsorption and desorption experiments. The adsorption of  
349 RNZ on Coconut AC was at pH = 7, and the desorption step was at the same pH. The pH of  
350 the desorption step was not varied because the adsorption capacity of Coconut AC did not  
351 depend on the pH for equilibrium concentrations of RNZ less than 100 mg/g. In the case of  
352 DCF, the adsorption of DCF on Wood AC was carried out at pH = 6 and the desorption at  
353 pH = 11. These pH conditions were selected because the Wood AC exhibited the highest and  
354 lowest adsorption capacity at pH = 6 and pH = 11. The desorption equilibrium data of RNZ  
355 and DCF from the Coconut and Wood ACs are displayed in Figures 7a and 7b. The  
356 experimental data for adsorption and desorption steps are denoted by the letter A and D,  
357 respectively, and followed by the corresponding experiment number.

358 The desorption percentage, %Des, was assessed by the subsequent equation:

$$\%Des = \frac{q_o - q_{des,e}}{q_o - q_{des,rev}} \times 100 \% \quad (8)$$

359 where  $q_{d,rev}$  is the uptake of pharmaceutical adsorbed at the desorption equilibrium supposing  
360 that the adsorption is reversible, mg/g. The adsorption could be considered reversible if the  
361 %Des was equal to 100 %. Contrarily, the adsorption would be irreversible when %Des was  
362 less than 100 %. The  $q_{des,rev}$  was computed by solving the Langmuir isotherm and equation  
363 (2) representing the desorption mass balance.



364 Figure 7a displays that the desorption equilibrium data D3, D4 and D5 are above the  
365 adsorption isotherm at pH = 7, demonstrating that the adsorption of RNZ on Coconut is not  
366 reversible. The %Des of RNZ adsorbed on Coconut AC were 80, 71 and 72 % for the  
367 experiments D3, D4 and D5 so less than 29 % of RNZ did not desorb and remained adsorbed.  
368 This result reveals that one of the adsorption mechanisms of RNZ is not reversible.

369 The %Des of DCF adsorbed on Wood AC were 100 and 98 % for the experiments D1  
370 and D2, correspondingly, and as shown in Figure 7b, the desorption experimental data D1  
371 and D2 were on the adsorption isotherm at pH = 11. Thus, the adsorption of DCF on Wood  
372 AC was reversible, corroborating that the predominant adsorption mechanisms of DCF on  
373 Wood AC are the electrostatic attractions and the  $\pi$ - $\pi$  dispersion interactions.

374 After the desorption experiment, the capacity of the regenerated ACs for adsorbing  
375 pharmaceuticals was evaluated to analyze the reuse of the regenerated ACs. The re-  
376 adsorption efficiency %RE was calculated employing equation (3) and ranged between 72  
377 and 77 % for DCF adsorbed on Wood AC at pH = 6, whereas the %RE for RNZ adsorbed on  
378 Coconut AC varied from 17 to 22 % at pH = 7. Thus, the regeneration of the CAs saturated  
379 with the pharmaceutical was adequate for the Wood AC but not for Coconut AC. Another  
380 regeneration method, such as microwave or thermal treatment, has to be investigated.

### 381 **3.7 Effect of temperature on the capacity of Coconut and Wood ACs for adsorbing RNZ** 382 **and DCF**

383 The influence of temperature on the uptake of RNZ and DCF adsorbed on Coconut  
384 and Wood ACs at pH = 7 is depicted in Fig. 8. For an RNZ equilibrium concentration of 400  
385 mg/L (See Fig. 8a), the uptake of RNZ adsorbed on Coconut AC was promoted and non-  
386 influenced by incrementing the temperature from 15 to 25 °C and 25 to 35 °C, respectively.  
387 A comparable tendency was also noted for the adsorption of RNZ on an AC commercially

388 known as Filtrasorb 400 when the temperature varied from 10 to 40 °C (Moral-Rodríguez et  
 389 al. 2016). The mass of RNZ adsorbed at 35, 25 and 15 °C was 408, 403 and 352 mg/g,  
 390 correspondingly indicating that the capacity of Coconut AC increased 14.5 % when the  
 391 temperature rose from 15 to 25 °C. Likewise, Fig. 8b shows that the adsorption of DCF was  
 392 significantly influenced by increasing the temperature from 15 to 25 and slightly augmented  
 393 from 25 to 35 °C. For a DCF concentration of 400 mg/g, the uptakes of DCF adsorbed were  
 394 363, 413 and 427 mg/g at 15, 25 and 35 °C. These outcomes verified that the adsorption  
 395 capacity of Wood AC towards DCF was raised 14 % and 3.4 % while incrementing the  
 396 temperature from 15 to 25 °C and 25 to 35 °C.

397 The isosteric adsorption heat,  $(\Delta H_{ads})_q$ , for RNZ and DCF, was estimated using the  
 398 experimental data at 15 and 25 °C since the adsorption capacity varied in this temperature  
 399 range. The  $(\Delta H_{ads})_q$  was estimated employing the following equation (Leyva-Ramos 1989):

$$(\Delta H_{ads})_q = \frac{R \ln \frac{C_2}{C_1}}{\frac{1}{T_2} - \frac{1}{T_1}} \quad (4)$$

400 where  $(\Delta H_{ads})_q$  is the isosteric adsorption enthalpy, J/mol; R is the gas law constant, 8.314  
 401 J/K mol;  $C_2$  and  $C_1$  are the equilibrium concentrations of the pharmaceutical at temperatures  
 402  $T_2$  and  $T_1$ , correspondingly, and at the same mass of the pharmaceutical adsorbed at  
 403 equilibrium (q), mg/L;  $T_2$  and  $T_1$  are the temperatures at the conditions 2 and 1, respectively,  
 404 K.

405 The  $\Delta H_{ads}$  was estimated to be 56.5 and 56.3 kJ/mol for the adsorption of RNZ on  
 406 Coconut AC at  $q = 358$  mg/g, and DCF on Wood AC at  $q = 372$  mg/g, correspondingly. Thus,  
 407 the adsorption of both pharmaceuticals was endothermic. It is worthwhile to mention that the  
 408  $\Delta H_{ads}$  decreased drastically as the  $q$  was reduced because the experimental adsorption  
 409 equilibrium data were overlapped for  $q$  less than 270 mg/g.

#### 410 4. CONCLUSIONS

411 Coconut, Wood, Merck, Norit and Darco ACs presented different textural and  
412 physicochemical properties. The  $S_{\text{BET}}$  varied from 510 to 1357  $\text{m}^2/\text{g}$ , and the cumulative  
413 volume of micropores ranged from 34 to 86 %. The Wood AC had an acid character, whereas  
414 the Coconut AC showed a basic character. The Coconut AC exhibited the highest adsorption  
415 capacity towards RNZ (444  $\text{mg}/\text{g}$ ), while the Wood AC showed the maximum mass of DCF  
416 adsorbed (405  $\text{mg}/\text{g}$ ) from water solutions.

417 The surface area, as well as the acid sites concentration, significantly influenced the  
418 adsorption capacity of all ACs, corroborating that the predominant adsorption mechanism  
419 was the  $\pi$ - $\pi$  stacking interactions. Besides, in the pH span of 3-7, the electrostatic interactions  
420 did not affect the adsorption of RNZ on Coconut AC; however, the hydrophobic interactions  
421 favored the adsorption of RNZ at pH = 11. In contrast, the capacity of Wood AC for DCF  
422 was reduced by the electrostatic repulsion occurring between the negatively charged surface  
423 of the AC and the anionic DCF.

424 The desorption results revealed that the adsorption of DCF on Wood AC was  
425 reversible, whereas that of RNZ on Wood AC was not. The uptake of RNZ adsorbed on  
426 Coconut AC and DCF adsorbed on Wood AC was lessened by diminishing the temperature  
427 from 25 to 15  $^{\circ}\text{C}$ ; hence, the adsorption of RNZ and DCF was endothermic in this  
428 temperature range. However, it remained nearly constant, incrementing the temperature from  
429 25 and 35  $^{\circ}\text{C}$ .

430 The adsorption on ACs is a feasible process for efficiently removing RNZ and DCF  
431 from aqueous solutions, but the textural and chemical properties must be considered in  
432 selecting the proper commercial AC.

433

434 **ACKNOWLEDGMENT**

435 E. Mendoza-Mendoza thanks for the financial support to CONACyT through the  
436 Catedras program, project No. 864. This study was financially supported by Fondo de Apoyo  
437 a la Investigación (FAI)-Universidad Autonoma de San Luis Potosi (UASLP), through grant  
438 No.: C20-FAI-10-27.27.

439

440 **DECLARATIONS**

441 **Authors' contributions** AIMR carried out data curation, methodology, investigation,  
442 writing-original draft preparation and visualization. RLR performed funding acquisition,  
443 investigation, project administration, supervision, methodology, writing, reviewing and  
444 editing. EMM accomplished conceptualization, supervision, methodology, writing,  
445 reviewing and editing. PEDF engaged in methodology, writing-original draft preparation and  
446 visualization. DHCA participated in data curation, methodology and writing-original draft  
447 preparation. MFAF carried out methodology, investigation and characterization of activated  
448 carbons. CFG performed methodology, investigation and characterization of activated  
449 carbons.

450 **Availability of data and materials:** Datasets used during the current study and  
451 supplementary data are available from the corresponding author on reasonable request.

452 **Compliance with ethical standards**

453 **Ethics approval and consent to participate:** Not applicable.

454 **Consent for publication:** No applicable.

455 **Competing interests:** The authors declare that they have no competing interests.

456

457

458 **REFERENCES**

- 459 Babić BM, Milonjić SK, Polovina MJ, Kaludierović BV (1999) Point of zero charge and  
460 intrinsic equilibrium constants of activated carbon cloth. *Carbon*.  
461 [https://doi.org/10.1016/S0008-6223\(98\)00216-4](https://doi.org/10.1016/S0008-6223(98)00216-4)
- 462 Boehm HP (1966) Chemical identification of surface groups. *Adv Catal*.  
463 [https://doi.org/10.1016/S0360-0564\(08\)60354-5](https://doi.org/10.1016/S0360-0564(08)60354-5)
- 464 Brunauer S, Emmett PH, Teller E (1938) Adsorption of gases in multimolecular layers. *J Am*  
465 *Chem Soc*. <https://doi.org/10.1021/ja01269a023>
- 466 Carrales-Alvarado DH, Ocampo-Pérez R, Leyva-Ramos R, Rivera-Utrilla J (2014) Removal  
467 of the antibiotic metronidazole by adsorption on various carbon materials from aqueous  
468 phase. *J Colloid Interface Sci*. <https://doi.org/10.1016/j.jcis.2014.08.023>
- 469 Chianese S, Iovino P, Canzano S et al (2016) Ibuprofen degradation in aqueous solution by  
470 using UV light. *Desalin Water Treat*. <https://doi.org/10.1080/19443994.2016.1153908>
- 471 Díaz-Cruz MS, García-Galán MJ, Barceló D (2008) Highly sensitive simultaneous  
472 determination of sulfonamide antibiotics and one metabolite in environmental waters by  
473 liquid chromatography-quadrupole linear ion trap-mass spectrometry. *J Chromatogr A*.  
474 <https://doi.org/10.1016/j.chroma.2008.03.029>
- 475 Dos Reis GS, Bin Mahbub MK, Wilhelm M et al (2016) Activated carbon from sewage  
476 sludge for removal of sodium diclofenac and nimesulide from aqueous solutions. *Korean J*  
477 *Chem Eng*. <https://doi.org/10.1007/s11814-016-0194-3>
- 478 Gómez MJ, Martínez Bueno MJ, Lacorte S et al (2007) Pilot survey monitoring  
479 pharmaceuticals and related compounds in a sewage treatment plant located on the  
480 Mediterranean coast. *Chemosphere*. <https://doi.org/10.1016/j.chemosphere.2006.07.051>

481 Halling-Sørensen B, Nors Nielsen S, Lanzky PF et al (1998) Occurrence, fate and effects of  
482 pharmaceutical substances in the environment- A review. *Chemosphere*.  
483 [https://doi.org/10.1016/S0045-6535\(97\)00354-8](https://doi.org/10.1016/S0045-6535(97)00354-8)

484 Jeon J, Hollender J (2019) In vitro biotransformation of pharmaceuticals and pesticides by  
485 trout liver S9 in the presence and absence of carbamazepine. *Ecotoxicol Environ Saf*.  
486 <https://doi.org/10.1016/j.ecoenv.2019.109513>

487 Kümmerer K (2009) Antibiotics in the aquatic environment - A review - Part I. *Chemosphere*.  
488 <https://doi.org/10.1016/j.chemosphere.2008.11.086>.

489 Leyva- Ramos R (1989) Effect of temperature and pH on the adsorption of an anionic  
490 detergent on activated carbon. *J Chem Technol Biotechnol*.  
491 <https://doi.org/10.1002/jctb.280450308>

492 Leyva-Ramos R (2007) Importancia y aplicaciones de la adsorción en fase líquida. In:  
493 Moreno-Piraján JM(ed) *Sólidos porosos, Preparación, Caracterización y Aplicaciones*.  
494 Ediciones Uniandes, Bogotá, Colombia, pp 155-211.

495 Lin AYC, Yu TH, Lin CF (2008) Pharmaceutical contamination in residential, industrial, and  
496 agricultural waste streams: Risk to aqueous environments in Taiwan. *Chemosphere*.  
497 <https://doi.org/10.1016/j.chemosphere.2008.08.027>

498 Lin AYC, Tsai YT (2009) Occurrence of pharmaceuticals in Taiwan's surface waters: Impact  
499 of waste streams from hospitals and pharmaceutical production facilities. *Sci Total Environ*.  
500 <https://doi.org/10.1016/j.scitotenv.2009.03.009>

501 Llinàs A, Burley JC, Box KJ et al (2007) Diclofenac solubility: Independent determination  
502 of the intrinsic solubility of three crystal forms. *J Med Chem*.  
503 <https://doi.org/10.1021/jm0612970>

504 Malhotra M, Suresh S, Garg A (2018) Tea waste derived activated carbon for the adsorption  
505 of sodium diclofenac from wastewater: adsorbent characteristics, adsorption isotherms,  
506 kinetics, and thermodynamics. *Environ Sci Pollut Res.* [https://doi.org/10.1007/s11356-018-](https://doi.org/10.1007/s11356-018-3148-y)  
507 3148-y

508 Martínez-Costa JI, Maldonado Rubio MI, Leyva-Ramos R (2020) Degradation of emerging  
509 contaminants diclofenac, sulfamethoxazole, trimethoprim and carbamazepine by bentonite  
510 and vermiculite at a pilot solar compound parabolic collector. *Catal Today.*  
511 <https://doi.org/10.1016/j.cattod.2018.07.021>

512 Méndez-Díaz JD, Prados-Joya G, Rivera-Utrilla J et al (2010) Kinetic study of the adsorption  
513 of nitroimidazole antibiotics on activated carbons in aqueous phase. *J Colloid Interface Sci.*  
514 <https://doi.org/10.1016/j.jcis.2010.01.089>

515 Moral-Rodríguez AI, Leyva-Ramos R, Ocampo-Pérez R et al (2016) Removal of ronidazole  
516 and sulfamethoxazole from water solutions by adsorption on granular activated carbon:  
517 equilibrium and intraparticle diffusion mechanisms. *Adsorption.*  
518 <https://doi.org/10.1007/s10450-016-9758-0>

519 Moral-Rodríguez AI, Leyva-Ramos R, Ania CO et al (2019) Tailoring the textural properties  
520 of an activated carbon for enhancing its adsorption capacity towards diclofenac from aqueous  
521 solution. *Environ Sci Pollut Res.* <https://doi.org/10.1007/s11356-018-3991-x>

522 Moreno-Castilla C (2004) Adsorption of organic molecules from aqueous solutions on  
523 carbon materials. *Carbon.* <https://doi.org/10.1016/j.carbon.2003.09.022>

524 Richard H.D, Mycek M.J, Harvey R.A, Champe P.C (2007) *Lippincott's Illustrated Reviews:*  
525 *Pharmacology.* Lippincott Williams & Wilkins.

526 Rouquerol F, Rouquerol J, Sing KSW et al (2014) *Adsorption by powders and porous solids:*  
527 *Principles, methodology and applications.* Academic Press, France.

528 Santos LHMLM, Gros M, Rodriguez-Mozaz S et al (2013) Contribution of hospital effluents  
529 to the load of pharmaceuticals in urban wastewaters: Identification of ecologically relevant  
530 pharmaceuticals. *Sci Total Environ.* <https://doi.org/10.1016/j.scitotenv.2013.04.077>

531 Spongberg AL, Witter JD (2008) Pharmaceutical compounds in the wastewater process  
532 stream in Northwest Ohio. *Sci Total Environ.*  
533 <https://doi.org/10.1016/j.scitotenv.2008.02.042>

534 Ternes TA, Hirsch R (2000) Occurrence and behavior of X-ray contrast media in sewage  
535 facilities and the aquatic environment. *Environ Sci Technol.*  
536 <https://doi.org/10.1021/es991118m>

537 Viotti PV, Moreira WM, dos Santos OAA et al. (2019) Diclofenac removal from water by  
538 adsorption on *Moringa oleifera* pods and activated carbon: Mechanism, kinetic and  
539 equilibrium study. *J Clean Prod.* <https://doi.org/10.1016/j.jclepro.2019.02.129>

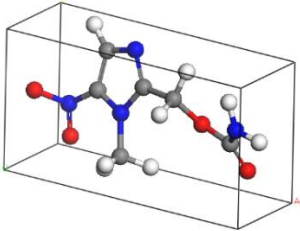
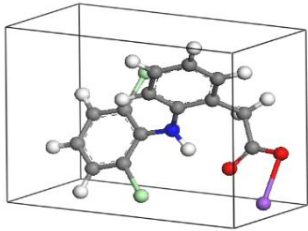
540 Wang J, Wang S (2016) Removal of pharmaceuticals and personal care products (PPCPs)  
541 from wastewater: A review. *J. Environ. Manage.* 182:620–640.  
542 <https://doi.org/10.1016/j.jenvman.2016.07.049>.

543 Watkinson AJ, Murby EJ, Kolpin DW, Costanzo SD (2009) The occurrence of antibiotics in  
544 an urban watershed: From wastewater to drinking water. *Sci Total Environ.*  
545 <https://doi.org/10.1016/j.scitotenv.2008.11.059>

546



**Table 1.** Molecular structure and physicochemical properties of RNZ and DCF.

Compound	Molecular structure	Molecular Weight (g/mol)	Dimensions		
			X, Y, Z (nm)	pK <sub>ow</sub>	pK <sub>a</sub>
Ronidazole C <sub>6</sub> H <sub>8</sub> N <sub>4</sub> O <sub>4</sub> (RNZ)		200.15	X: 0.913 Y: 0.448 Z: 0.264	0.38	pK <sub>a1</sub> : 1.32 pK <sub>a2</sub> : 12.99
Diclofenac sodium C <sub>14</sub> H <sub>10</sub> Cl <sub>2</sub> NNaO <sub>2</sub> (DCF)		318.13	X: 0.960 Y: 0.708 Z: 0.472	3.91	pK <sub>a</sub> : 4.0

550

**Table 2.** Textural properties of the commercial ACs.

<b>AC</b>	<b>S<sub>BET</sub></b> <b>(m<sup>2</sup>/g)</b>	<b>V<sub>P</sub><sup>a</sup></b> <b>(cm<sup>3</sup>/g)</b>	<b>d<sub>P</sub><sup>b</sup></b> <b>(nm)</b>	<b>V<sub>mic</sub><sup>c</sup></b> <b>(cm<sup>3</sup>/g)</b>	<b>L<sub>0</sub><sup>d</sup></b> <b>(nm)</b>	<b>S<sub>mic</sub></b> <b>(m<sup>2</sup>/g)</b>
Wood	1357	1.18	3.51	0.40	1.41	746
Merck	1074	0.57	2.13	0.33	1.27	554
Coconut	960	0.44	1.81	0.38	0.97	800
Norit	646	0.55	3.43	0.28	0.93	433
Darco	510	0.58	5.34	0.21	1.22	328

551 <sup>a</sup> Total pore volumen552 <sup>b</sup> Average pore diameter553 <sup>c</sup> Micropore volume554 <sup>d</sup> Micropore average width

555

556

557

**Table 3.** The concentration of acidic and basic sites of the commercial ACs.

<b>Activated Carbon</b>	<b>Total acid sites (meq/g)</b>	<b>Total basic sites (meq/g)</b>
Coconut	0.711	4.995
Merck	0.093	0.093
Darco	0.141	0.093
Norit	0.313	1.366
Wood	1.874	0.243

558

559

560

561 **Table 4.** Parameter values of the Prausnitz-Radke adsorption isotherms for the adsorption of  
 562 RNZ and DCF in aqueous solution on ACs at T = 25 °C and pH = 7.

<b>Compound</b>	<b>AC</b>	<b>a (L/g)</b>	<b>b (L<sup>β</sup>/mg<sup>β</sup>)</b>	<b>β</b>	<b>%D</b>
RNZ	Wood	50.3	0.46	0.81	3.7
	Merck	46.5	0.51	0.83	0.9
	Coconut	55.6	0.42	0.80	8.0
	Norit	165	1.26	0.89	4.4
	Darco	188	3.01	0.82	4.6
DCF	Wood	29.2	0.10	0.92	9.9
	Merck	104	1.30	0.82	10.5
	Coconut	709	6.70	0.88	14.1
	Norit	104	1.30	0.82	4.9
	Darco	5.41	0.05	0.90	1.8

563

564

565

566

567

568 **Table 5.** Parameters of the **Prasnitz-Radke** adsorption isotherms for the adsorption of RNZ  
 569 on Coconut and DCF on Wood from aqueous solution at different operating conditions and  
 570 I = 0.01 N.

571

Operating Conditions		RNZ on Coconut				DCF on Wood			
T (°C)	pH	<i>a</i> (L/g)	<i>b</i> (Lβ/mgβ)	β	%D	<i>a</i> (L/g)	<i>b</i> (Lβ/mgβ)	β	%D
25	6					114	0.26	0.95	15
25	7	55.6	0.42	0.80	8.0	29.2	0.10	0.92	9.9
25	9	313	2.55	0.78	21	36.3	0.17	0.94	1.4
25	11	27.9	0.20	0.75	2.5	119	1.15	0.84	3.1
15	7	84.2	0.63	0.84	9.0	22.7	0.23	0.78	19
35	7	167	1.34	0.80	1.0	23.7	0.06	0.97	2.0

572

573

574

575 List of Figure Captions

576 **Fig. 1** Speciation diagrams of 1a) RNZ and 1b) DCF in aqueous solution as a function of the  
577 solution pH.

578 **Fig. 2** Adsorption isotherms of a) RNZ and b) DCF at pH = 7 on ACs at T = 25 °C and I =  
579 0.01 N. The lines represent the predictions of the Radke-Prausnitz isotherm.

580 **Fig. 3** Effect of surface area on the adsorption capacity of the ACs.

581 **Fig. 4** Dependence of the adsorption capacity of ACs on the concentrations of the acidic sites per  
582 unit of surface area.

583 **Fig. 5** Effect of solution pH on the adsorption isotherm of RNZ on Coconut AC at T = 25  
584 °C and I = 0.01 N. The lines were predicted with the Radke-Prausnitz model.

585 **Fig. 6** Effect of solution pH on the adsorption isotherm of DCF on Wood AC at T = 25 °C  
586 and I = 0.01 N. The lines show the prediction of the Radke-Prausnitz isotherm.

587 **Fig. 7** Adsorption and desorption equilibrium data of pharmaceuticals on ACs at T = 25°C.  
588 a) Adsorption (pH = 7) and desorption (pH = 7) of RNZ on Coconut AC, and b) Adsorption  
589 (pH = 6) and desorption (pH = 11) of DCF on Wood AC. The lines represent the Radke-  
590 Prausnitz isotherm.

591 **Fig. 8** Effect of temperature on the adsorption isotherms of a) RNZ on Coconut AC and b) DCF on  
592 Wood AC at pH = 7 and I = 0.01 N. The lines represent the isotherm of the Radke-Prausnitz model.

593

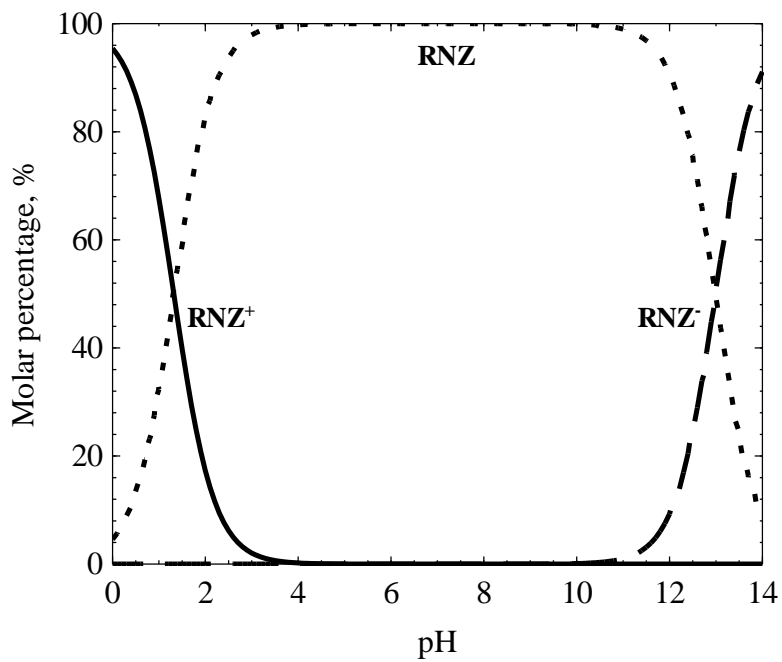
594

595

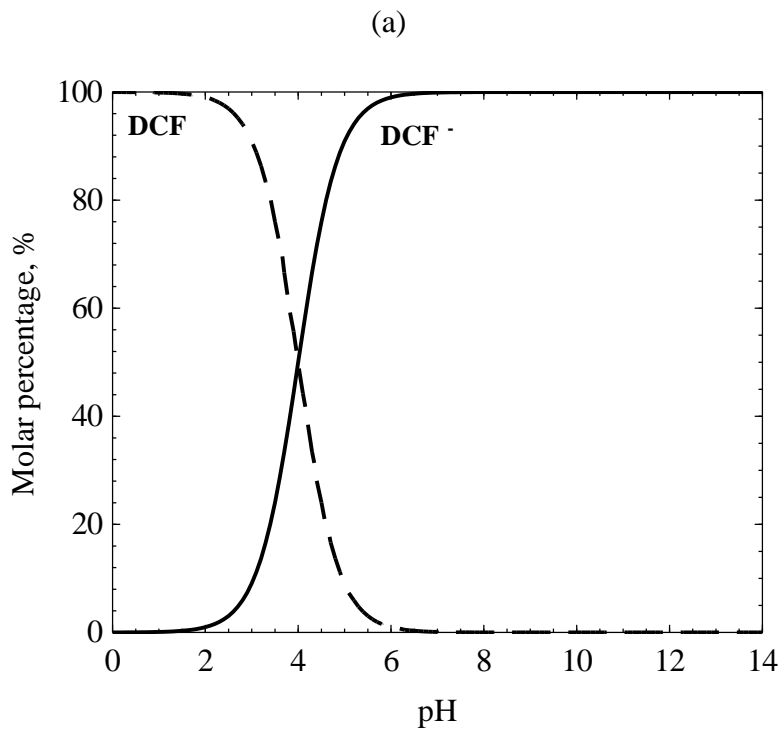
596

597

598



599



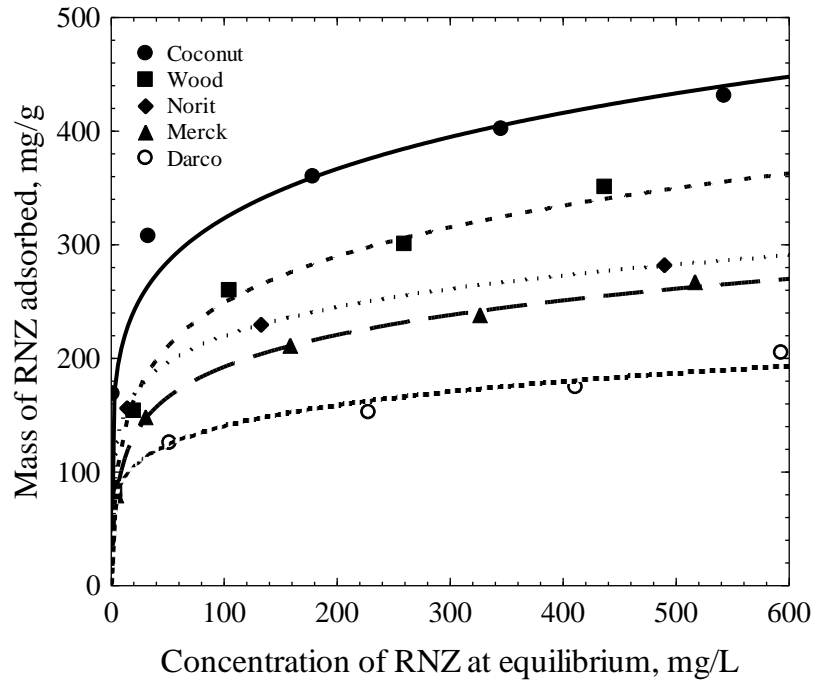
600

601 **Fig. 1**

602

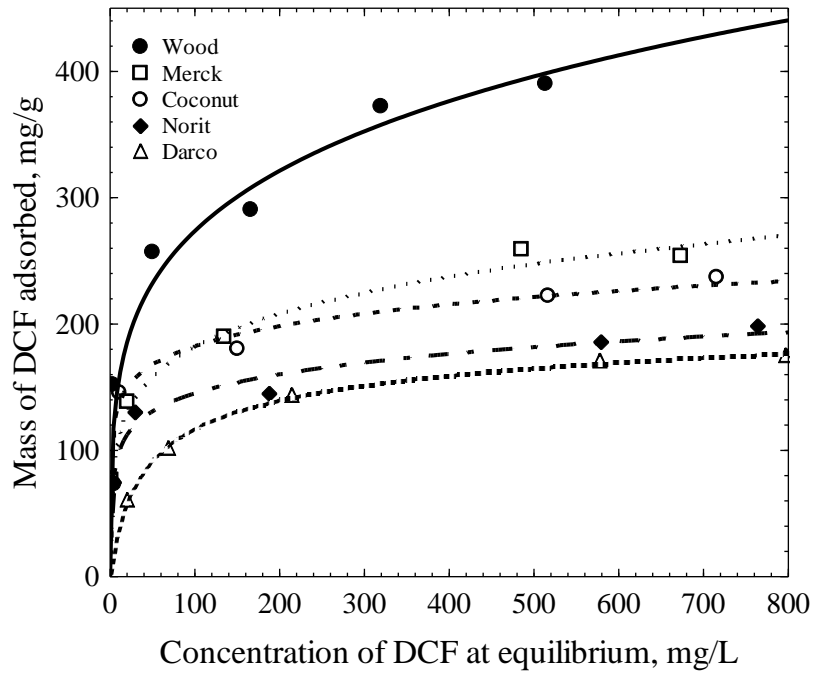
603

604



605

(a)



606

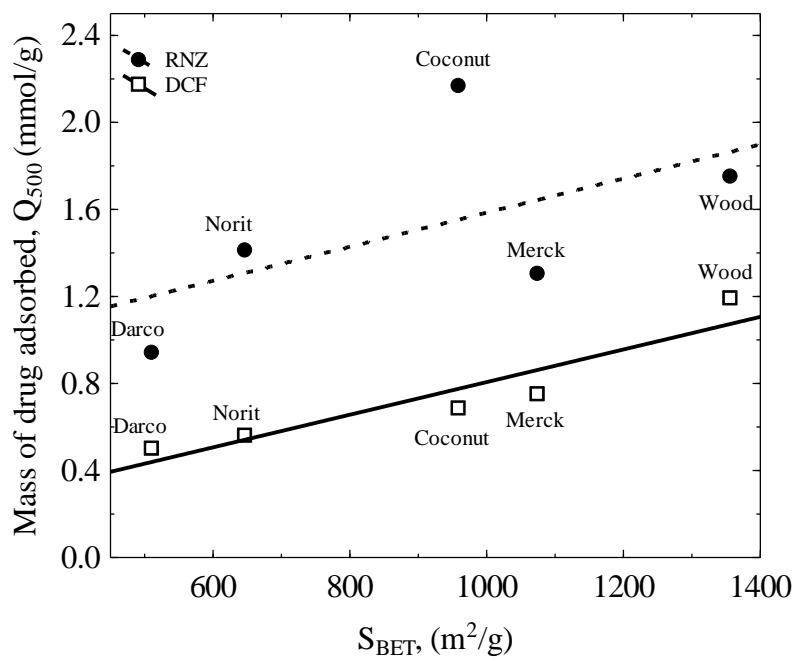
(b)

607 Fig. 2

608



609



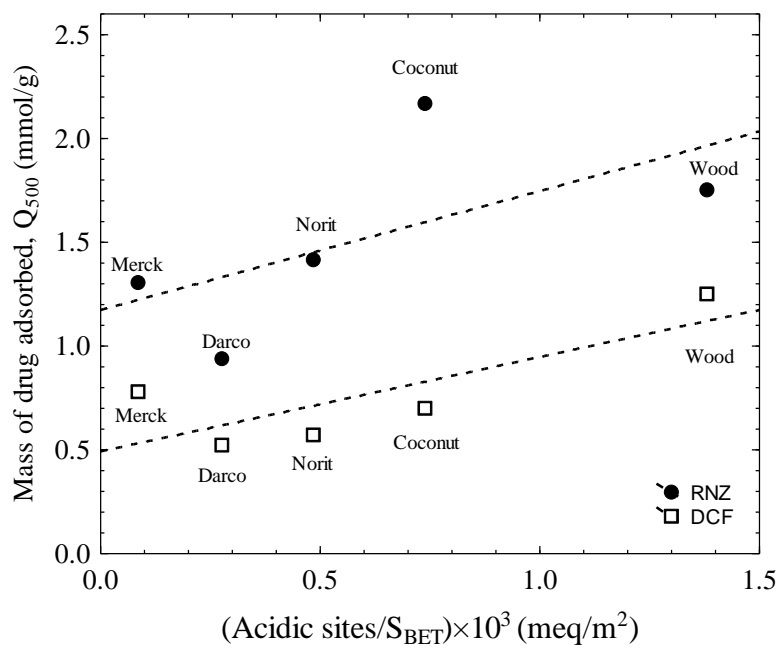
610

611 **Fig. 3**

612

613

614



615

616

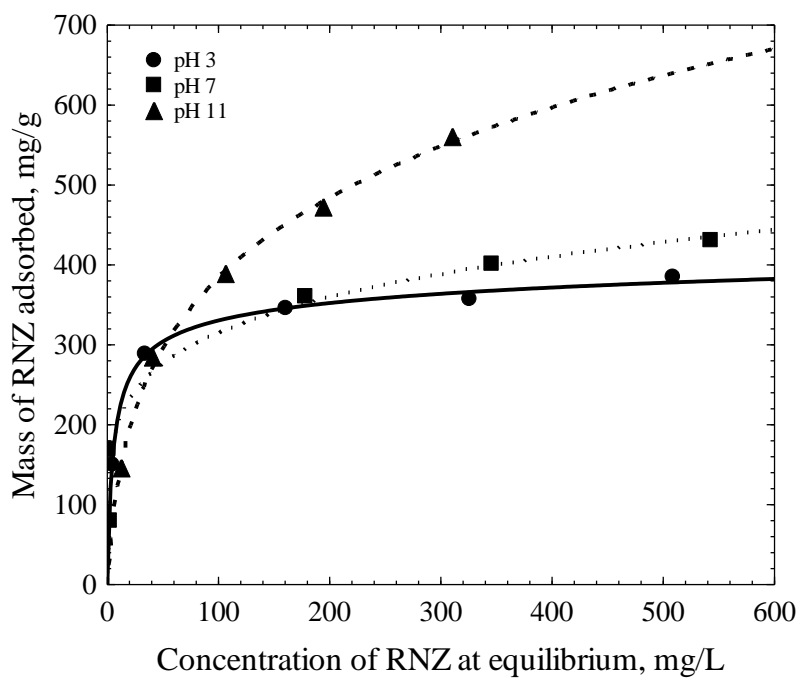
617 **Fig. 4**

618

619

620

621



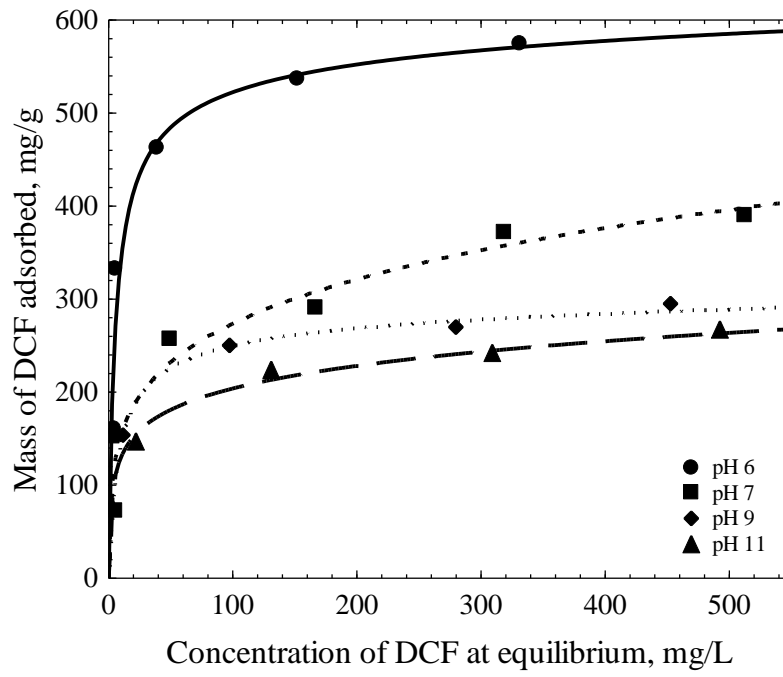
622

623 **Fig. 5**

624

625

626



627

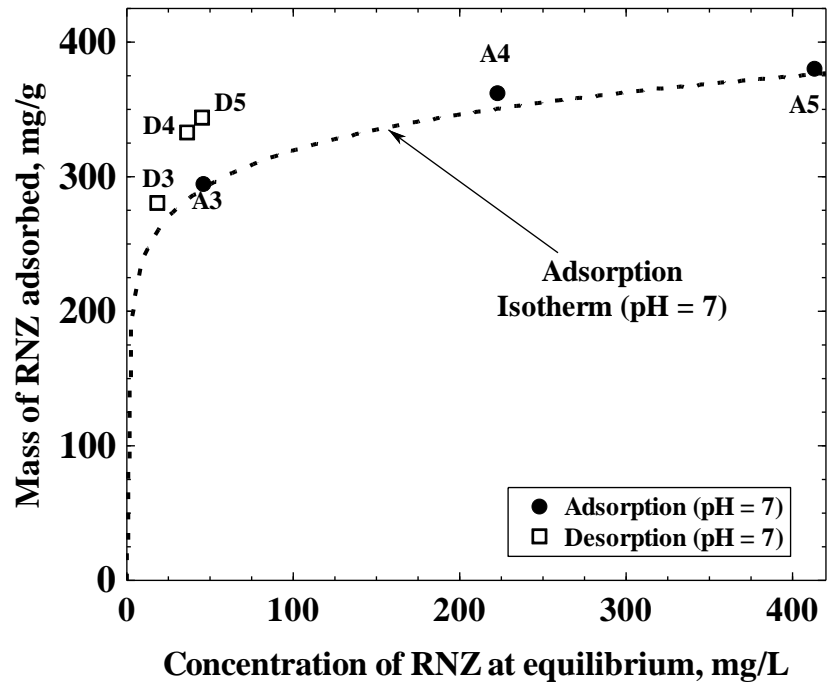
628 **Fig. 6**

629

630

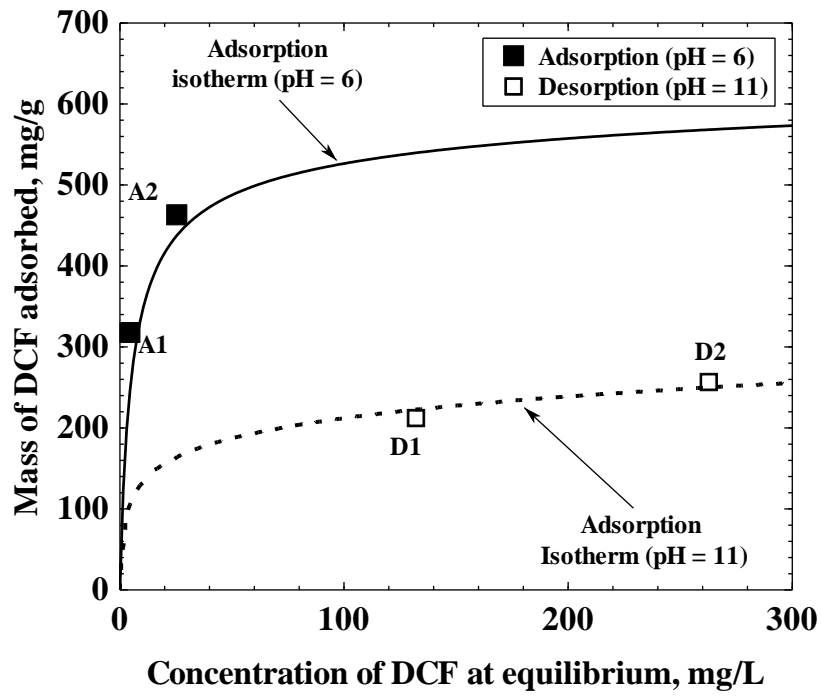
631

632



633

a)

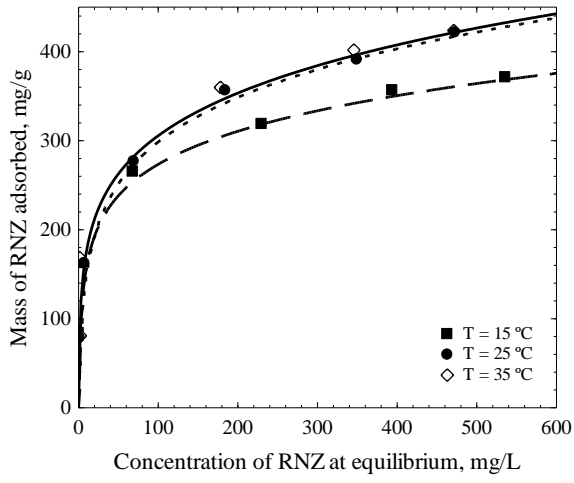


634

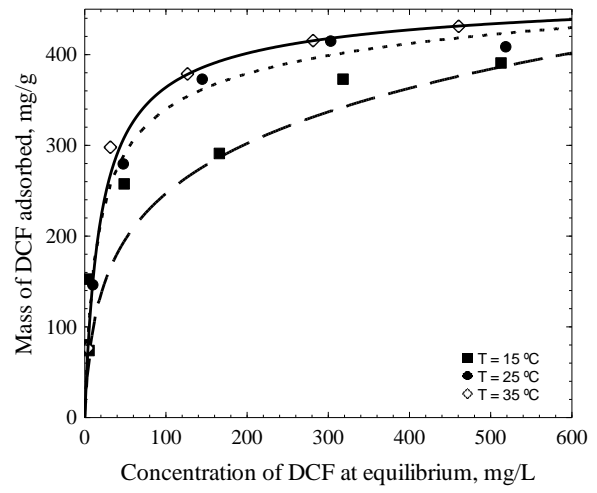
b)

635 **Fig. 7**

636



(a)



(b)

637

638 **Fig. 8**

639

640